Engineering Failure Analysis 79 (2017) 198–207

Contents lists available at ScienceDirect

Engineering Failure Analysis

journal homepage: www.elsevier.com/locate/engfailanal

The role of microstructure and grain orientations on intergranular cracking susceptibility of UNS 17400 martensitic stainless steel

Mohammad Masoumi[a], Sérgio Souto Maior Tavares[b], Juan Manuel Pardal[b], Tabatta Regihna Brito Martins[b], Marcelo José Gomes da Silva[a,*], Hamilton Ferreira Gomes de Abreu[a]

[a] Universidade de São Paulo, Escola Politécnica, Departamento de Engenharia Metalúrgica e de Materiais, Av. Professor Mello Moraes, 2463, CEP 05508-030 São Paulo, Brazil

[b] Universidade Federal Fluminense, Departamento de Engenharia Mecânica, Rua Passo da Pátria, 156, CEP 22245-110, Niterói, RJ, Brazil

ARTICLE INFO

Keywords:
17–4 pH steel
Crystallographic orientation
Hydrogen cathodic charging
Intergranular cracking susceptibility

ABSTRACT

The aim of this work was to investigate the role of crystallographic orientations and grain boundary characteristics as a new approach to controlling the intergranular cracking (IGC) susceptibility. In this respect, hydrogen cathodic charging under two different current densities was carried out on 17–4 pH steel (H900 condition) in order to search for correlations between intergranular corrosion and microstructure, inclusions, and grain orientations. Then, to emphasize the importance of crystallographic orientation in IGC, hydrogen cathodic charging was carried out on 17–4 pH steel in solution condition, in which grains oriented with {110} and {111} parallel to the normal direction (ND) are dominant. The results showed that a reduction in the fraction of undesired {001}//ND grains and development of {110}, {112}, and {111}//ND texture components improved the IGC resistance. In addition, a higher fraction of low angle and special boundaries with low internal energy due to better compatibility between adjacent grains was observed in the uncracked sample and led to increased IGC resistance.

1. Introduction

UNS S17400 (17–4 pH martensitic stainless) steel is widely used in various applications such as in the marine construction, petrochemical, oil, and nuclear industries due to its excellent combination of mechanical properties and corrosion resistance. Therefore, much attention has been paid to investigation of the effect of solution annealing and ageing behaviour of 17–4 pH steel over recent decades [1–3]. This steel can be purchased with different final heat treatments, including H900, which consists of solution treatment at 1040 °C followed by ageing at 482 °C (900 °F) for 1 h. Another option is H1100, which is a solution treatment at the same temperature combined with over-ageing at 593 °C (1100 °F) for 4 h [1]. The increasing demand for particular applications in harsh and corrosive environments has forced the steelmaking industry to improve the mechanical and corrosion properties. Intergranular cracking (IGC) is one of the most critical damage modes in the development of 17–4 pH steel [1]. Because of the harmful effect of IGC in high strength steels, numerous investigations have been performed [4–6]. Researchers have suggested several methods to reduce the probability of IGC such as adding micro-alloying elements [7,8], eliminating precipitations [9], and reducing segregations [10,11]. These strategies have not always been effective. Therefore, control of the crystallographic textures and grain

* Corresponding author at: Universidade Federal do Ceará, Departamento de Engenharia Metalúrgica e de Materiais, Campus Universitário do Pici - Bloco 729, CEP 60440-554 Fortaleza, CE, Brazil.
E-mail address: mgsilva@ufc.br (M.J. Gomes da Silva).

http://dx.doi.org/10.1016/j.engfailanal.2017.04.008
Received 9 June 2016; Received in revised form 3 April 2017; Accepted 15 April 2017
Available online 21 April 2017
1350-6307/

boundary characteristics has recently been proposed as a new approach to reduce the susceptibility to hydrogen embrittlement (HE) and can be effective in these steels.

In steels, carbon and nitrogen with a small atomic radius tend to occupy the octahedral positions in the body-centred cubic (BCC) lattice [12]. This lattice distortion in the structure leads to weakening of the covalent atomic bonds, especially in {001} planes with a small number of nearest neighbours and low packing density. As a result, grains with {001} orientation are prone to crack formation and failure behaviour [13]. Meanwhile grains oriented in the {111} and {110} directions corresponding to dense planes in BCC structure show higher corrosion resistance [14,15]. Moreover, Schreiber et al. [16] studied the anodic dissolution of iron in crystal scale. They reported that the maximum dissolution rate occurs in grain oriented with {100} parallel to the normal direction ({001}// ND), while {111} and {110}//ND showed higher resistance to dissolution during electrochemical corrosion. On the other hand, high-angle grain boundaries (HAGBs), having high stored energy, provide an easier path for crack propagation. Meanwhile, a coincidence site lattice (CSL) and low angle grain boundaries (LAGBs) with better fit between the adjacent lattices and lower stored energy are considered as obstacles to crack propagation, leading to a reduction in the crack growth rate [17,18].

Since the H900 condition is common for applications requiring high strength and corrosion resistance, improvements in corrosion resistance have always drawn attention. In this work, a 17–4 pH high-strength martensitic stainless steel was solution-annealed at 1040 °C for 1 h followed by ageing at 482 °C for 1 h. Then, the samples were subjected to hydrogen cathodic charging in acid solution under two different current densities, 30 and 300 mA/cm^2. Although IGC was formed in both samples, the cracked and uncracked regions were studied to find a correlation between the microstructure and microtexture and the IGC susceptibility. Then, hydrogen cathodic charging was carried out in the same solution heat treatment following by ageing at 600 °C, which led to the same microstructure with dominant {110} and {111}//ND grain orientations, highlighting the importance of crystallographic orientations in IGC. The result showed an excellent increase in IGC resistance.

2. Experimental procedures

The chemical composition of 17–4 pH steel used in this work is given in Table 1. Two specimens (10 mm thick) were cut from a cylindrical bar 25.4 mm in diameter. The samples were solution treated at 1040 °C followed by ageing at 482 °C (900 °F) for 1 h. After that, the samples were embedded in resin with a copper wire for electric contact, ground with emery paper, and polished with 1-μm alumina paste. This electrode was subjected to hydrogen cathodic charging in 1 M H_2SO_4 solution with 0.3 g/l of As_2O_3. Two experiments were conducted with current densities of 30 and 300 mA/cm^2. After charging for 24 h at room temperature, the specimens were lightly polished with 1-μm alumina paste and then etched with Vilella's reagent (90 ml of ethanol, 10 ml of HCl, and 1 g of picric acid) and observed in a scanning electron microscope (SEM) equipped with energy dispersive x-ray analysis (EDX).

The electron backscatter diffraction (EBSD) measurements were carried out with an Oxford Channel 5 system attached to an FEI XL-30 SEM operating at an acceleration voltage of 20 kV, sample tilt angle of 70°, working distance of 12 mm, and step size of 0.5 μm. In the EBSD measurements, the grain orientations, grain boundary distributions, and Taylor factor were analyzed by the Oxford Instruments Channel 5 and MTEX-Free and Open Source Software Toolbox [19]. Grain boundary misorientation in this study was defined as (i) a dislocation tangle with point-to-point misorientation of less than 2°, (ii) LAGBs with misorientation between 2 and 15°, (iii) HAGBs with point-to-point misorientation greater than 15°, and (iv) special grain boundaries (Σ - CSL). Also, the deformation texture was simulated through Taylor type models using HKL Technology Channel 5.

3. Results and discussion

Fig. 1 shows the SEM micrographs of the H900 specimens. A martensitic structure with hardness of around 496 ± 5 HV was found in these samples. Moreover, a remarkable amount of Nb carbides were observed in this condition (Fig. 1b). The Nb carbides were distributed throughout the martensitic lath boundaries and in the prior austenite grain boundaries. The formation of NbC enhances the strength without significant loss of ductility and toughness [20]. Also, small and spherical niobium nitrides, (Nb, Ti)N, are identified by EDX examination as illustrated in Fig. 2. Recently, Tavares et al. [21] studied the Nb carbides in H900 condition and reported that this condition is not sensitized because of the low amount of chromium carbides in grain boundaries. However, it was shown that NbC precipitations were not able to prevent IGC by applying a cathodic current in hydrogenation tests.

In order to study the effect of microstructure, inclusions, and grain orientations on IGC, the samples were subjected to hydrogen cathodic charging in acid solution under two different current densities: 30 and 300 mA/cm^2. Fig. 3 shows the polarization curve of specimens in the same hydrogenation solution. In this curve, the open circuit potential (E_{OCP}) was − 0.42 V_{SCE} and the potentials corresponding to current densities of 30 and 300 mA/cm^2 were − 0.58 and − 0.95 V_{SCE}, respectively. These potentials were maintained during the experiments on cathodic hydrogenation.

Fig. 4a and b presents micrographs of the samples just after cathodic charging with H_2SO_4 solution with the addition of As_2O_3 and the application of current densities of 30 and 300 mA/cm^2, respectively. The micrographs demonstrate that under both current

Table 1
Chemical composition of the 17–4 pH steel (wt%).

C	Mn	Cr	Ni	Si	P	S	Nb	Cu
0.029	0.82	15.67	4.22	0.30	0.022	0.016	0.166	3.320

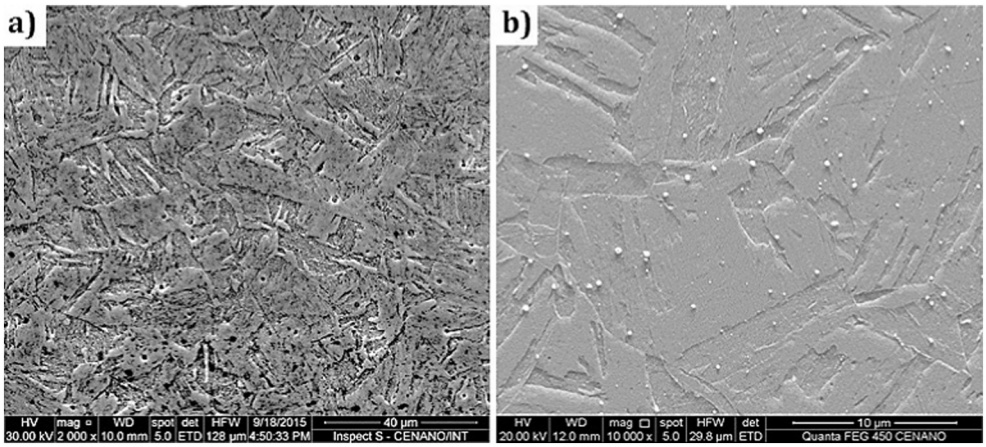

Fig. 1. SEM micrographs of the H900 specimens, (a) × 2000 and (b) × 10,000.

densities, the samples suffered from intergranular attacks, and the martensitic structure is highly susceptible to IGC. The intergranular cracks and pores shown in these images are typical of hydrogen embrittlement (HE). The results showed a direct relation between applied current density and IGC susceptibility, in good agreement with the findings of other researchers [22,23], who have reported that increasing hydrogen-trapped solubility and decreasing diffusivity caused more hydrogen entrapment in steel and boosted cracking susceptibility.

Fig. 4 shows the typical HIC crack propagation by joining of micro-cracks. It is worth mentioning that IGC susceptibility depends on segregation bands and the size and morphology of inclusions. Segregation zones were not found in the samples, and thus their effect could be ignored. It is well known that the presence of inclusions due to precipitation-hardening facilitates IGC cracking. On the other hand, the defects and inclusions trap the atomic hydrogen, and since the hydrogen content reaches a critical value, the internal stress due to recombination of two hydrogen atoms into a hydrogen molecule can initiate cracks without applying an external stress. EDX examinations were carried out in some crack regions to determine the role of inclusions in IGC, and the results are presented in Fig. 5. A typical MnS inclusion was found to be the nucleation site for crack formation.

Besides, in some regions, cracks nucleated and propagated without the presence of inclusions. Therefore, EBSD analyses were carried out to find the correlations between IGC susceptibility, grain orientations, and grain boundary distributions in the vicinity of cracks for both specimens. In this respect, normal-direction inverse pole figure (IPF) maps of different regions that were located far enough apart to eliminate mutual effects were analyzed to study the cracked and uncracked regions in both samples. The related IPF maps are shown in Fig. 6, and the LAGBs and HAGBs are identified by thin and thick black lines. Complex behaviors of crack propagation during hydrogenation tests such as multiple crack nucleation sites, crack branching, stepwise crack propagation, and crack arrest were observed in samples. This highlighted the importance of understanding the role of grain orientation in IGC

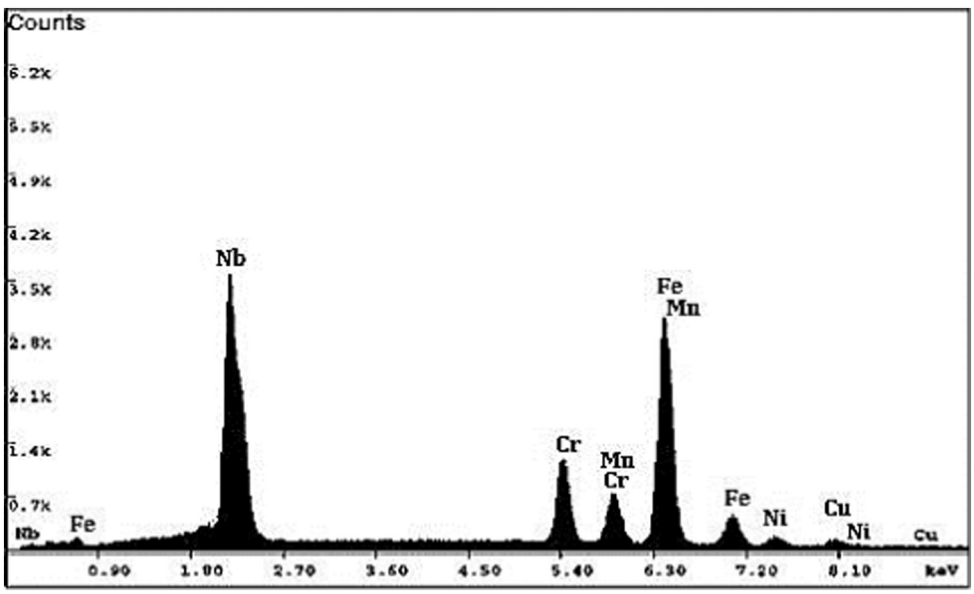

Fig. 2. EDX examination of small and spherical particles in H900 condition.

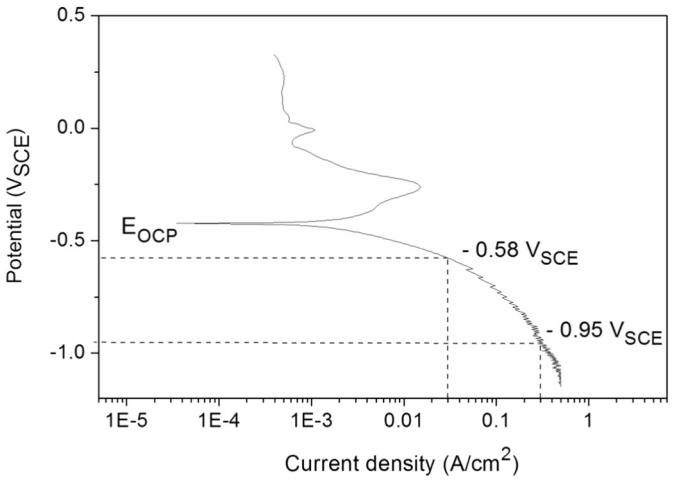

Fig. 3. Polarization curve in 1 M H_2SO_4 solution with 0.3 g/L of As_2O_3 solution showing potentials corresponding to 30 and 300 mA/cm^2.

corrosion. Intergranular cracks nucleated inside the grains oriented with {001}//ND (red color) are presented in Fig. 5a. In addition, as shown in Fig. 5b, cracks also tended to propagate along boundaries associated with {100}//ND texture components. Poor resistance to IGC corrosion would be obtained in the presence of grains oriented with {001} parallel to the normal direction. Conversely, a reduction in its volume fraction and development of desired texture components with more corrosion resistance can improve IGC resistance.

In order to evaluate the effect of grain orientations on enhancing and decreasing crack formation, the fraction of grain orientation intensity in some main orientations was calculated with 2.5° deflection of the ideal orientation, as shown in Fig. 7. From the results, it can be understood that in both regions (a) and (c) in which cracks propagated, the fraction of undesired {001} grains parallel to the normal direction is dominant. Meanwhile, an increase in the number of grains associated with more dense planes such as {110}, {112}, and {111} parallel to the normal direction enhanced the IGC resistance. However, the effect of grains related to RD fibre ({110}//RD, rolling direction) and TD fibre ({110}//TD transverse direction) directions is not clear.

It is well-known that once a crack has nucleated, it tends to propagate along the weak grain boundaries [24]. As mentioned earlier, the behaviour of a boundary against a crack tip depends on the crystallographic orientations of the neighboring grains associated with the boundary. Although the IPF orientation map is an excellent method of presenting grain orientation, there is an unavoidable limitation in the total Euler scheme [25]. To help compensate for this limitation the orientation distribution function (ODF) was calculated and shown in Fig. 8 to find a correlation between crack behaviors and grain orientations.

The grain orientation analyses showed that grains oriented with {001}//ND texture fibre, especially in (001)[$\bar{1}\,\bar{5}$0], (001)[1$\bar{1}$0], and (001)[$\bar{1}\,\bar{1}$0], were highly susceptible to IGC in both samples (Fig. 8a, c). The results are entirely compatible with the findings of Venegas [26] and Schreiber [27], who studied the relationship between crystallographic texture and pitting corrosion. They reported that the grains lying in the {001} direction parallel to the normal direction are highly susceptible to pitting corrosion. Moreover, the formation of (112)[$\bar{1}\,\bar{7}$4] texture components is shown in Fig. 8c. In BCC structure, shear bands can form inside the grains because of rearrangement by dislocation motion in {112} planes, corresponding to close-packed planes [28]. Thus, the crack branching and

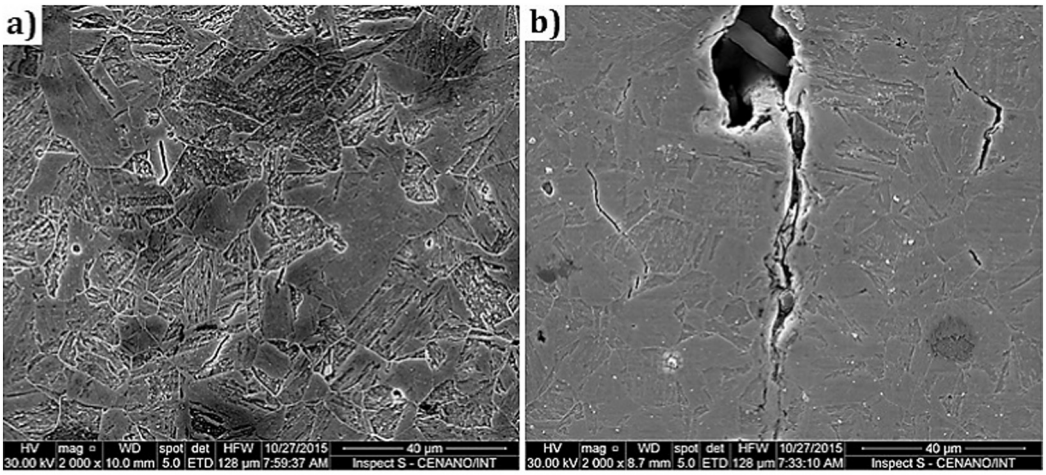

Fig. 4. Micrographs of samples after hydrogenation with H_2SO_4 with As_2O_3 solution by applying current densities of a) 30 and b) 300 mA/cm^2.

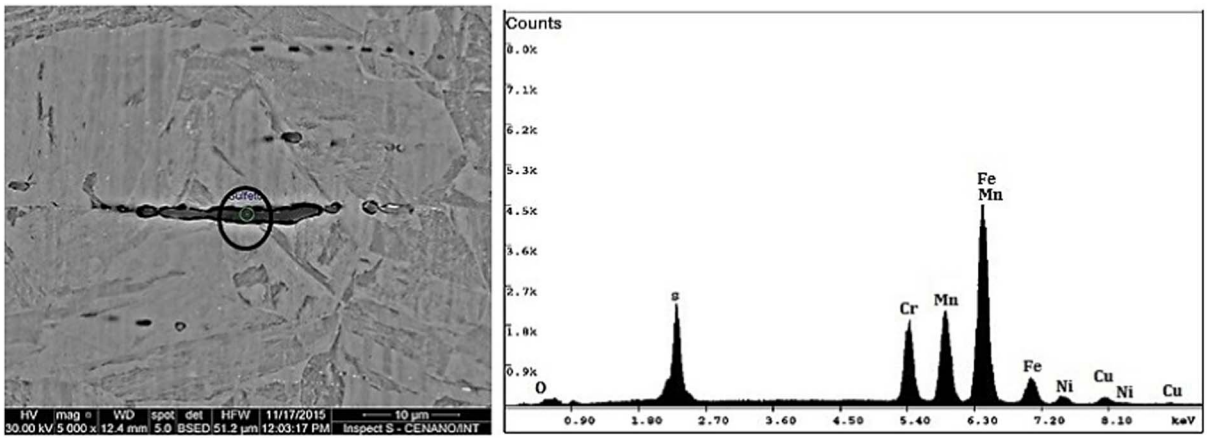

Fig. 5. EDX analyses for inclusions in crack propagation.

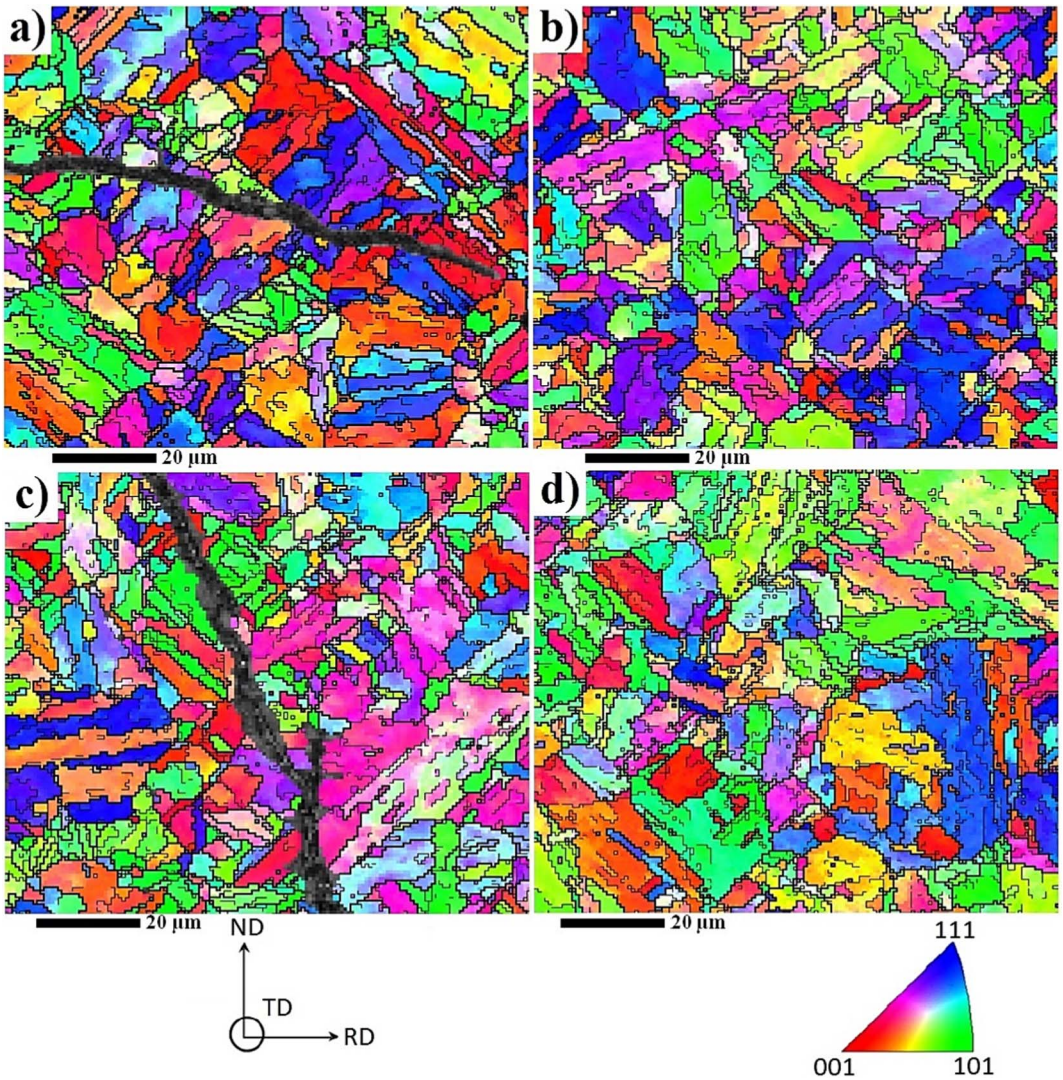

Fig. 6. IPF maps for current densities of (a, b) 30 and (c, d) 300 mA/cm^2.

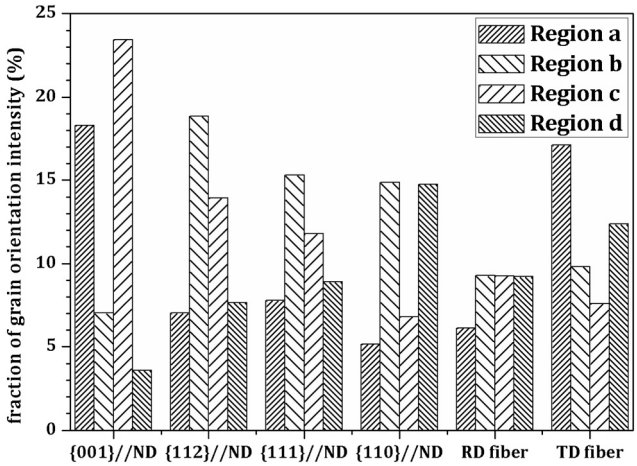

Fig. 7. Fraction of grain orientation intensity in main fibres.

stepwise propagation which are shown in IPF maps are probably associated with this phenomenon. On the other hand, uncracked regions in both samples after hydrogenation demonstrated a minimum number of grains with {001}//ND orientations, instead of significant development in {112}, {111}, and {110}//ND fibres. The (112)[2$\bar{4}$1] and ($\bar{1}$12)[201] components, as well as the {111} and {110}//ND fibres, were dominant in these regions. As a consequence, higher IGC resistance was obtained in these regions.

Furthermore, it is believed that the intergranular cracks tend to propagate along the grain boundaries. It is well known that during hydrogen charging, hydrogen atoms produced in the cathode are adsorbed on the surface. Part of the hydrogen is absorbed and

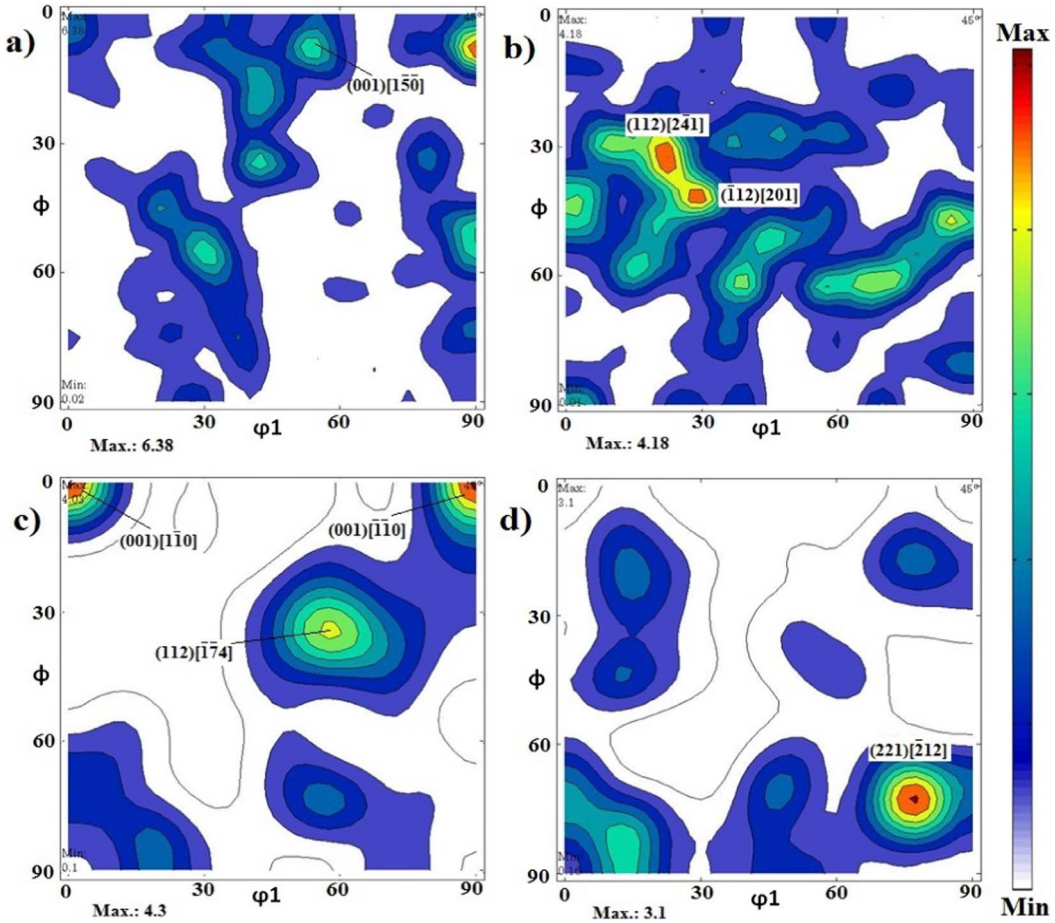

Fig. 8. The related ODFs for current densities of (a, b) 30, and (c, d) 300 mA/cm^2.

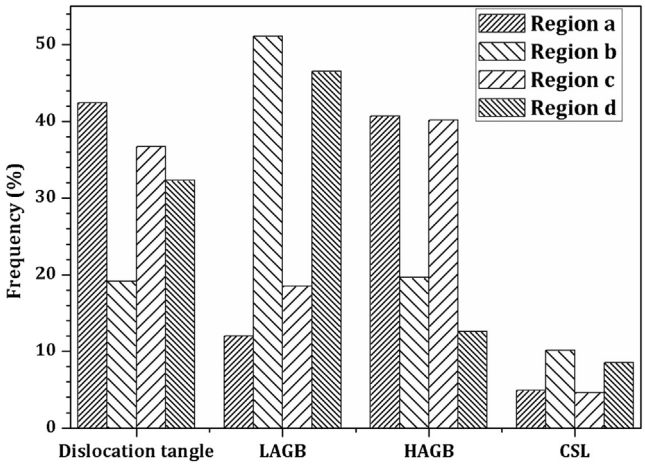

Fig. 9. Grain boundary distributions in samples under current densities of both cracked and uncracked regions after hydrogenation.

diffused in the steel, where it can be trapped. The microstructure has a significant number of trapping sites such as inclusions and HAGBs with high misorientation angles between adjacent grains, which may have higher hydrogen solubility [29]. In this regard, the understanding of the behaviour of crack propagation in the case of different types of grain boundaries is essential. Grain boundary distributions obtained with each IPF are shown in Fig. 9. It is observed that the volume fractions of dislocation tangles and HAGBs in cracked regions in both samples are significantly higher than in the uncracked areas. It is worth mentioning that the EBSD technique cannot detect dislocation, while the variation in the crystal orientation of an individual grain is brought about by stored dislocations generated during recombination of nascent hydrogen into molecular hydrogen [30]. In general, dislocation tangles and HAGBs with

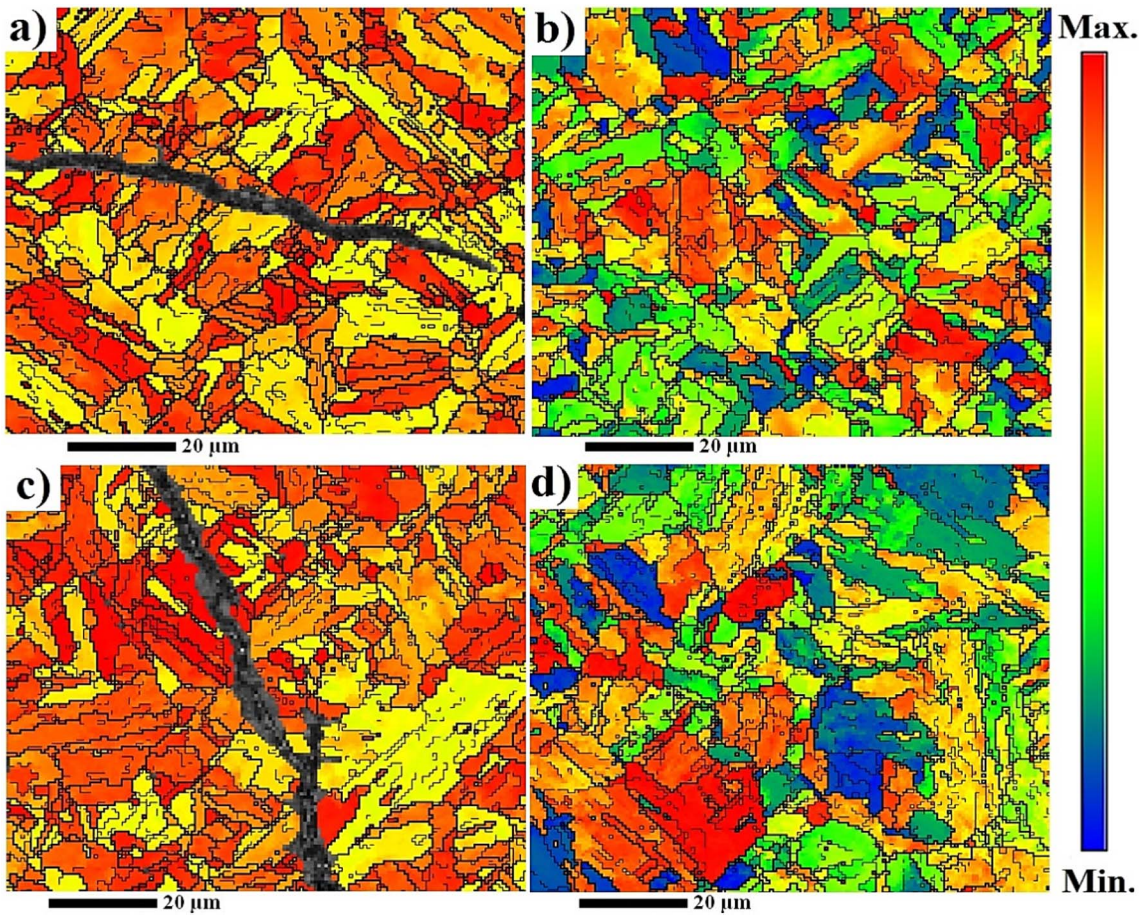

Fig. 10. Taylor factor maps for current densities of (a, b) 30 and (c, d) 300 mA/cm^2.

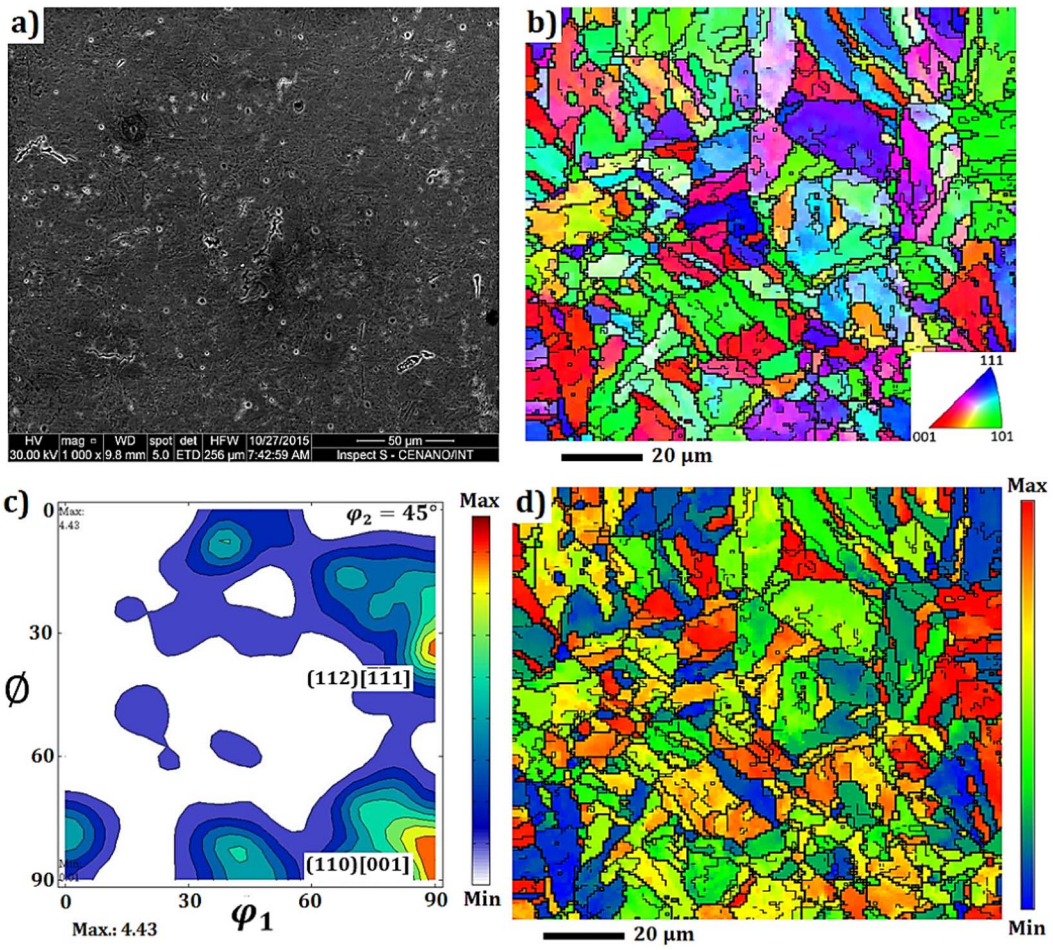

Fig. 11. (a) SEM micrograph, (b) normal direction IPF, (c) ODF, and (d) Taylor factor map of sample aged at 600 °C following hydrogen cathodic charging with a current density of 300 mA/cm^2.

high stored energy and incompliant lattice arrangement enhance the high internal stress, facilitating crack formation. When the internal stress reaches the critical amount, crack nucleation and propagation occur as shown in the cracked sample (Fig. 6a and c). On the other hand, the higher fraction of LAGBs and CLS boundaries with low internal energy due to better compatibility between adjacent grains observed in the uncracked regions led to improved IGC resistance in the sample.

The crystallographic analysis of EBSD maps led to other interesting microstructural interpretations regarding the prediction of grain orientation resistance against hydrogen embrittlement state [31]. In this respect, the grains are categorized into three main groups. In the first group, shown in blue color, the grains are already aligned in the stress corrosion state and favourable crystal direction, which can easily provide enough slip systems for dislocation movement. These are considered as soft grains. The second group comprises the grains that can arrange adequate slip systems by rotation in an appropriate direction. In the third and last group, the hard grains with insufficient slip systems and conditions to rotate are indicated in red in Taylor factor maps [32,33]. As a consequence, dislocation pileup and stress concentration develop, especially near the boundaries of these grains, leading to crack formation. As mentioned earlier, the {001}//ND grains formed in the cracked sample were not able to provide enough slip systems. Conversely, the grains oriented with {112}, {111}, and {110}//ND close to close-packed planes in BCC structure with a low Taylor factor reduced the local plastic deformation by facilitating the dislocation movements and led to increases in crack resistance in this specimen (Fig. 10). As shown in Fig. 10a and c, a high Taylor factor value due to high dislocation accumulation and insufficient slip systems for dislocation movement provided a driving force for crack nucleation or facilitation of crack propagation. Meanwhile, uncracked regions with a lower Taylor factor are not prone to IGC (Fig. 10b, d). Githinji et al. [34] also reported that a very low local misorientation value due to low strain with low dislocation density causes the low Taylor factor. In other words, an increasing contribution of multiple slip systems homogeneously distributed in the grains and at grain boundaries results in a higher uniform elongation.

In order to verify the role of crystallographic orientations and grain boundary characteristics in IGC resistance, another sample of the same material was solution treated at 1040 °C followed by ageing at 600 °C (1112 °F) for 1 h [35] (as the minimum temperature required to reach the austenite phase). Then, the sample was subjected to hydrogen cathodic charging with a current density of

300 mA/cm^2. Although the final microstructure was quite similar to the others, the specimen exhibited a significant improvement in intergranular corrosion. The microstructure, normal direction IPF, Taylor factor map, and ODF analyses after hydrogen cathodic charging are presented in Fig. 11. Grain orientations associated with TD fibre ({110}//TD) such as (112)[$\bar{1}\,\bar{1}$1] and (110)[001] components were predominant in this condition (Fig. 11c), which is near to the close-packed slip systems in a cubic lattice. Calculation of the grain boundary distributions showed that the fractions of dislocation tangles and HAGBs changed to about ~20.32% and ~53.13%, respectively. This demonstrates that static recrystallization took place and new strain-free grains developed in this condition. Moreover, the Taylor factor map (Fig. 11d) shows the significant low-Taylor-factor grain distributions in the final microstructure, which means there is a uniform dislocation distribution, preventing the formation of local stress concentration and increasing the IGC resistance.

4. Conclusions

Since the use of UNS 17400 martensitic stainless steel is common for applications requiring high strength and corrosion resistance, improvements in corrosion resistance have always drawn attention. In this work, cathodic hydrogenation charging tests with two different current densities were carried out in H900 condition to determine the role of microstructure and grain orientations in intergranular cracking (IGC) susceptibility. Poor resistance to IGC was obtained in the presence of grains oriented with {001} parallel to the normal direction. Then, hydrogen cathodic charging was carried out with the same solution heat treatment following by ageing at 600 °C and yielded the same microstructure, with dominant grain orientations of {110} and {111}//ND, highlighting the importance of crystallographic orientations in IGC. The results exhibited an excellent increase in IGC resistance. In addition, a very low local misorientation value (low dislocation tangle) due to low strain with low dislocation density caused a low Taylor factor, which improved the IGC resistance.

References

[1] R.D.K. Misra, C.Y. Prasad, T.V. Balasubramanian, P. Rama Rao, Effect of post-aging quenching treatment on impact toughness of 17-4 precipitation hardened stainless steel, Scr. Mater. 22 (8) (1988) 1323–1325.
[2] R.H. Shay, R.A. Puerta, D.A. Domchek, Advances in hydrogen usage in the metals and electronics industries, Int. J. Hydrog. Energy 9 (6) (1984) 539–542.
[3] L.W. Tsay, W.C. Lee, R.K. Shiue, J.K. Wu, Notch tensile properties of laser-surface-annealed 17-4 PH stainless steel in hydrogen-related environments, Corros. Sci. 44 (9) (2002) 2101–2118.
[4] H.A. Acciari, A.C. Guastaldi, M.A. Christopher, On the development of the electrochemical potentiokinetic method, Electrochim. Acta 46 (25) (2001) 3867–3877.
[5] D.C.S. Garcia, R.N. Carvalho, V.F.C. Lins, D.M. Rezende, D.S. Dos Santos, Influence of microstructure in the hydrogen permeation in martensitic-ferritic stainless steel, Int. J. Hydrog. Energy 40 (47) (2015) 17102–17109.
[6] M. Asgari, R. Johnsen, A. Barnoush, Nanomechanical characterization of the hydrogen effect on pulsed plasma nitrided super duplex stainless steel, Int. J. Hydrog. Energy 38 (35) (2013) 15520–15531.
[7] G. Biggiero, A. Borruto, F. Gaudino, Embrittlement due to hydrogen in ferritic and martensitic structural steels, Int. J. Hydrog. Energy 20 (2) (1995) 133–139.
[8] M. Xiaoping, W. Lijun, V. Sundaresa, L. Chunming, Studies on Nb microalloying of 13Cr super martensitic stainless steel, Metall. Mater. Trans. A 43 (12) (December 2012) 4475–4486.
[9] Pierre-Jean Cunat, Alloying elements in stainless steel and other chromium-containing alloys, Euro Inox, Chromium Development Association, 2004, pp. 1–24.
[10] M. Monnot, R.P. Nogueira, V. Roche, G. Berthomé, E. Chauveau, R. Estevez, M. Mantel, Sulfide stress corrosion study of a super martensitic stainless steel in H2S sour environments: metallic sulfides formation and hydrogen embrittlement, Appl. Surf. Sci. 394 (1) (February 2017) 132–141.
[11] J.I.A.N.G. Wen, Z.H.A.O. Kun-yu, Y.E. Dong, L.I. Jun, S.U. Jie, Effect of heat treatment on reversed austenite in Cr15 super martensitic stainless steel, J. Iron Steel Res. Int. 20 (5) (May 2013) 61–65.
[12] A.M. Ilyin, Some features of grain boundary segregations in sensitized austenitic stainless steel, J. Nucl. Mater. 252 (2) (1998) 168–170.
[13] U.K. Viswanathan, G.K. Dey, M.K. Asundi, Precipitation hardening in 350 grade maraging steel, Metall. Mater. Trans. A 24 (1993) 2429–2442.
[14] V. Venegas, F. Caleyo, T. Baudin, J.H. Espina-Hernández, J.M. Hallen, On the role of crystallographic texture in mitigating hydrogen-induced cracking in pipeline steels, Corros. Sci. 53 (12) (2011) 4204–4212.
[15] M. Masoumi, L.P.M. Santos, I.N. Bastos, S.S.M. Tavares, M.J.G. da Silva, H.F.G. de Abreu, Texture and grain boundary study in high strength Fe–18Ni–Co steel related to hydrogen embrittlement, Mater. Des. 91 (2016) 90–97.
[16] M.A. Mohtadi-Bonab, J.A. Szpunar, R. Basu, M. Eskandari, The mechanism of failure by hydrogen induced cracking in an acidic environment for API 5L X70 pipeline steel, Int. J. Hydrog. Energy 40 (2) (2015) 1096–1107.
[17] A. Schreiber, C. Rosenkranz, M.M. Lohrengel, Grain-dependent anodic dissolution of iron, Electrochim. Acta 52 (27) (2007) 7738–7745.
[18] M.A. Mohtadi-Bonab, M. Eskandari, K.M.M. Rahman, R. Ouellet, J.A. Szpunar, An extensive study of hydrogen-induced cracking susceptibility in an API X60 sour service pipeline steel, Int. J. Hydrog. Energy 41 (7) (2016) 4185–4197.
[19] D. Raabe, S. Sandlöbes, J. Millán, D. Ponge, H. Assadi, M. Herbig, P.-P. Choi, Segregation engineering enables nanoscale martensite to austenite phase transformation at grain boundaries: a pathway to ductile martensite, Acta Mater. 61 (16) (2013) 6132–6152.
[20] F. Bachmann, R. Hielscher, H. Schaeben, Texture analysis with MTEX - free and open source software toolbox, Solid State Phenom. 160 (2010) 63–70.
[21] T. Depover, D. Pérez Escobar, E. Wallaert, Z. Zermout, K. Verbeken, Effect of hydrogen charging on the mechanical properties of advanced high strength steels, Int. J. Hydrog. Energy 39 (9) (2014) 4647–4656.
[22] S.S.M. Tavares, F.J. da Silva, C. Scandian, G.F. da Silva, H.F.G. de Abreu, Microstructure and intergranular corrosion resistance of UNS S17400 (17-4PH) stainless steel, Corros. Sci. 52 (11) (2010) 3835–3839.
[23] K. Matsumoto, Y. Kobayashi, K. Ume, K. Murakami, K. Taira, K. Arikata, Hydrogen induced cracking susceptibility of high-strength linepipe steels, Corros. Sci. 42 (6) (1986) 337–345.
[24] Z.Y. Liu, X.G. Li, C.W. Du, L. Lu, Y.R. Zhang, Y.F. Cheng, Effect of inclusions on initiation of stress corrosion cracks in X70 pipeline steel in an acidic soil environment, Corros. Sci. 51 (4) (2009) 895–900.
[25] T. Watanabe, S. Tsurekawa, The control of brittleness and development of desirable mechanical properties in polycrystalline systems by grain boundary engineering, Acta Mater. 47 (16) (1999) 4171–4185.
[26] W. Zhou, Z.L. Wang, Scanning microscopy for nanotechnology, Genet. Anal. Tech. Appl. 12 (2007) 41–75.
[27] V. Venegas, F. Caleyo, L.E. Vázquez, T. Baudin, J.M. Hallen, On the influence of crystallographic texture on pitting corrosion in pipeline steels, Int. J. Electrochem. Sci. 10 (2015) 3539–3552.
[28] A. Schreiber, C. Rosenkranz, M.M. Lohrengel, Grain-dependent anodic dissolution of iron, Electrochim. Acta 52 (27) (2007) 7738–7745.
[29] C. Cayron, Continuous atomic displacements and lattice distortion during fcc–bcc martensitic transformation, Acta Mater. 96 (2015) 189–202.

[30] M.A. Mohtadi-Bonab, M. Eskandari, K.M.M. Rahman, R. Ouellet, J.A. Szpunar, An extensive study of hydrogen-induced cracking susceptibility in an API X60 sour service pipeline steel, Int. J. Hydrog. Energy 41 (7) (2016) 4185–4197.
[31] M. Masoumi, C.C. Silva, M. Béreš, D.H. Ladino, H.F.G. Abreu, Role of crystallographic texture on the improvement of hydrogen-induced crack resistance in API 5L X70 pipeline steel, Int. J. Hydrog. Energy 42 (2) (2016) 1318–1326.
[32] U.F. Kocks, H. Mecking, Physics and phenomenology of strain hardening: the FCC case, Prog. Mater. Sci. 48 (3) (2003) 171–273.
[33] E. Demir, A Taylor-based plasticity model for orthogonal machining of single-crystal FCC materials including frictional effects, Int. J. Adv. Manuf. Technol. 40 (2009) 847–856.
[34] M.R. Stoudt, L.F. Levine, A. Creuziger, J.B. Hubbard, The fundamental relationships between grain orientation, deformation induced surface roughness and strain localization in an aluminum alloy, Mater. Sci. Eng. A 530 (2011) 107–116.
[35] D.N. Githinji, S. Northover, P.J. Bouchard, M.A. Rist, An EBSD study of the deformation of service-aged 316 austenitic steel, Metall. Mater. Trans. A 44 (9) (2013) 4150–4167.